





SLAB (ONE-TILE) SURFACE ENERGY BALANCE SCHEME: MODEL DESCRIPTION AND PRELIMINARY VALIDATION FOR AN URBAN SITE AND A WETLAND SITE

KRZYSZTOF FORTUNIAK¹ , MARIUSZ SIEDLECKI¹ , WŁODZIMIERZ PAWLAK¹ ,
JAN GÓROWSKI² 

Abstract. Adequate modelling of the heat balance of different surface types is key to improving high-resolution numerical weather forecasts. The problem is particularly relevant in urbanised areas, which, due to their significant accumulation of infrastructure and high population density, are particularly vulnerable to the effects of climate change. The paper presents an exhaustive description of the surface energy balance model developed by the Department of Meteorology and Climatology at the University of Lodz over the past two decades. The model uses a simple slab approach, wherein the canopy layer is regarded as a flat surface (a tile) with specific “bulk” physical parameters (radiative, aerodynamic, thermodynamic and hydrological). It was initially developed for use in urban areas, but since it is based on rather general parametrisations of surface–atmosphere fluxes, it can be applied to any land cover with specific “surface slab” parameters. Here we compare the model outputs with the measured flux data from two very distinct ecosystems: an urban setting and a wetland. Despite its simplicity, the model generally represents well the features of the heat balance of both wetlands and urban areas. The latent heat flux is best represented and the sensible heat flux and the radiation balance somewhat less well, probably due to the assumption that all energy exchange occurs on an infinitesimal flat active surface.

Key words: numerical modelling, surface energy balance, urban climate, wetlands

Introduction

Urban areas have become a subject of particular interest in the age of climate change (Rosenzweig *et al.* 2018). They occupy only about 3% of the Earth's land area (Nazarian *et al.* 2023), but contribute significantly to human impact on the climate. Urban agglomerations form “hot spots” on the map of greenhouse gas exchange, which contribute to more than 70% of global emissions (Lwasa *et al.* 2022; Seto *et al.* 2014). Furthermore, over half of the global population (~55%), resides in urban areas. In Europe, this

proportion is almost three-quarters (74%), while in Poland it stands at ~60%. At the same time, due to high population densities and substantial infrastructure accumulation, these areas are highly vulnerable to climate change (IPCC 2024). Serious risks may arise from the synergy of global effects with urban climate singularities. For example, the urban heat island (Oke 1973, 1982) can pose a particular threat to the health and even the lives of city dwellers during heat waves (Ho *et al.* 2023; Cheval *et al.* 2024). Improving the accuracy of urban weather and climate prediction is therefore critical to the protection of human health and the strengthening of urban resilience.

¹ University of Lodz, Faculty of Geographical Sciences, Institute of Climatology and Hydrology, Department of Meteorology and Climatology; Narutowicza 88 St., 90-139 Lodz; e-mail: krzysztof.fortuniak@geo.uni.lodz.pl, ORCID: 0000-0001-7043-8751; e-mail: mariusz.siedlecki@geo.uni.lodz.pl, ORCID: 0000-0002-5804-8985; e-mail: wlodzimierz.pawlak@geo.uni.lodz.pl, ORCID: 0000-0002-9785-4787

² University of Lodz, Doctoral School of Exact and Natural Sciences; Matejki 21/23 St., 90-237 Lodz; e-mail: jan.gorowski@edu.uni.lodz.pl, ORCID: 0000-0002-3660-803X

To achieve this goal, it is necessary to adequately model the surface–atmosphere heat, mass and momentum exchange at the urban scale (Grimmond *et al.* 2009; Lipson *et al.* 2023). Therefore, many research groups have recently been involved in developing models for parametrising the energy balance of urban surfaces. Models of considerable diversity in complexity have been developed that in disparate ways address city morphology, vegetative cover, radiation processes, turbulent fluxes, hydrological balance and the anthropogenic heat and moisture emission (Grimmond *et al.* 2009, 2010, 2011; Lipson *et al.* 2023).

The aim of this work is to characterise the surface energy balance model that has been developed in the Department of Meteorology and Climatology at the University of Lodz over the last two decades. The model, originally created in 2003 (Fortuniak 2003), was compared with others within the framework of the first International Project for the Comparison of Urban Land Surface Models (PILPS-Urban) (Grimmond *et al.* 2009, 2010, 2011) and more recently in the Urban-PLUMBER project (Lipson *et al.* 2023). The improvements made to the model over the past two decades, and the practical lack of a reasonably complete description of the model, led to the undertaking of this study.

The model was initially developed for use in urban areas, but since it is based on rather general parametrisations of surface–atmosphere fluxes, it can be applied to any land cover with specific “surface slab” parameters. To preliminarily evaluate the model's performance in very different ecosystems, we compare the results with flux data from two sites: an urban area and a wetland.

General model description, input and output variables

The model uses a simple slab approach, wherein the canopy layer is regarded as a flat surface (a tile) with specific “bulk” physical parameters (radiative, aerodynamic, thermodynamic and hydrological). No singularities of the surface geometry or physical processes within the canopy layer are taken into account. Similarly, the model does not explicitly consider vegetation coverage, but rather incorporates it into the parameters defining the canopy slab. The parameters of “urban slab” used in the model are:

C_g – heat capacity [$J \cdot m^{-3} \cdot K^{-1}$],
 k_g – thermal conductivity [$W \cdot m^{-1} \cdot K^{-1}$],

α – albedo, no snow,
 α_S – albedo, snow cover,
 ε – emissivity, no snow,
 ε_S – emissivity, snow cover,
 SMC_{min} – minimum soil moisture content,
 SMC_{max} – maximum soil moisture content,
 z_{0m} – roughness length for momentum [m].

Other input parameters are:

z_1 – effective level of forcing data
 $(z_1 = z_{data} - z_{displ.})$ [m],
 $Q_{Ant.}$ – anthropogenic heat flux [$W \cdot m^{-2}$] (optionally),
 P_{yr} – mean (climatological) annual precipitation total [m].

Forcing variables:

K_d – downward shortwave radiation [$W \cdot m^{-2}$],
 L_d – downward longwave radiation [$W \cdot m^{-2}$],
 T_{z1} – air temperature at level z_1 [K],
 q_{z1} – specific humidity of the air at level z_1 ,
 u_{z1} – wind speed at level z_1 [$m \cdot s^{-1}$],
 R_f – rainfall intensity [$kg \cdot m^{-2} \cdot s^{-1}$],
 S_f – snowfall intensity [$kg \cdot m^{-2} \cdot s^{-1}$].

For an energy balance defined in the form:

$$Q^* + Q_{Ant.} = Q_H + Q_E - Q_G \quad (1)$$

where: $Q^* = K_d - K_u + L_d - L_u$ is radiation balance, Q_H is sensible heat flux, Q_E is latent heat flux and Q_G is heat flux to the ground (surface slab), the model calculates upward shortwave, K_u , and longwave, L_u , radiation and the fluxes Q_H , Q_E and Q_G .

Radiation budget

The upward shortwave and longwave radiation is determined by the well-known equations:

$$K_u = K_d(1 - \alpha) \quad (2)$$

and

$$L_u = L_d(1 - \varepsilon) + \varepsilon \sigma T_{Surf}^4 \quad (3)$$

where σ is Stefan-Boltzmann constant and T_{Surf} is the surface temperature.

Temperature evolution of surface slab and heat flux to the ground

The temperature evolution in the vertical profile in the ground (surface slab), T_G , is determined

through the numerical solution of a one-dimensional heat diffusion equation:

$$\frac{\partial T_G}{\partial t} = v_g \frac{\partial^2 T_G}{\partial z^2} \quad (4)$$

with the Crank–Nicolson scheme employed for $n = 14$ levels with varying thicknesses: $d_i = 0.005, 0.01, 0.015, 0.02, 0.025, 0.03, 0.05, 0.1, 0.2, 0.5, 1.0, 3.0, 5.0$ and 10.0 m ($v_g = k_g/C_g$ is thermal diffusivity in $\text{m}^2 \cdot \text{s}^{-1}$). The bottom boundary conditions are defined by a constant temperature, which is taken to be equal to the mean annual air temperature for the location:

$$T_{G,n}(i+1) = T_{G,n}(i) = \text{const.} \quad (5)$$

where $T_{G,n}(i+1)$ and $T_{G,n}(i)$ represent the ground temperature of level n in iteration $i+1$ and in iteration i , respectively. The upper boundary conditions are defined by the surface energy balance, which can be expressed as:

$$\begin{aligned} & T_{G,1}(i+1) = \\ & = T_{G,1}(i) + \frac{\Delta t}{c_g d_1} (Q^* + Q_{\text{Ant.}} - Q_H - Q_E - Q_G) \end{aligned} \quad (6)$$

Finally, the Q_G is determined as:

$$Q_G = 2k_g \frac{(T_{G,1}(i) - T_{G,2}(i))}{(d_1 + d_2)} \quad (7)$$

Sensible heat and momentum flux

The sensible heat and momentum fluxes in the kinematic form are determined based on the concept of the friction velocity, u_* , and the temperature scale, T_* :

$$\overline{w'u'} = u_*^2 \quad (8)$$

$$\overline{w'T'} = -u_* T_* \quad (9)$$

The u_* and T_* are computed from the integrated flux profile relationship:

$$u_* = u_{z_1} \cdot k \left[\ln \left(\frac{z_1}{z_{0m}} \right) - \Psi_m \left(\frac{z_1}{L} \right) + \Psi_m \left(\frac{z_{0m}}{L} \right) \right]^{-1} \quad (10)$$

$$T_* = (T_{z_1} - T_{\text{Surf}}) \cdot k \left[\ln \left(\frac{z_1}{z_{0h}} \right) - \Psi_h \left(\frac{z_1}{L} \right) + \Psi_h \left(\frac{z_{0h}}{L} \right) \right]^{-1} \quad (11)$$

where Ψ_m and Ψ_h are integrals of the universal functions for momentum and heat, u_{z_1} [$\text{m} \cdot \text{s}^{-1}$] and T_{z_1} are the wind speed and air temperature at height z_1 , k is von Kármán constant (taken as 0.35). The surface temperature, T_{Surf} , is the temperature of the first ground level $T_{\text{Surf}} = T_{G,1}$.

The stability parameter, z_1/L , is found from its relation to the bulk Richardson number, defined in the model as:

$$Ri_b = gz(T_{z_1} - T_{\text{Surf}})/(T_{z_1} \cdot u_{z_1}^2) \quad (12)$$

In the case of a locally unstable situation ($Ri_b < 0$), the iterative solution of the relation:

$$z_1/L = Ri_b \frac{[\ln(\frac{z_1}{z_{0m}}) - \Psi_m(\frac{z_1}{L}) + \Psi_m(\frac{z_{0m}}{L})]^2}{[\ln(\frac{z_1}{z_{0h}}) - \Psi_h(\frac{z_1}{L}) + \Psi_h(\frac{z_{0h}}{L})]} \quad (13)$$

is used, whereas, for a stable case, the analytical form is applied from Mascart *et al.* (1995):

$$z_1/L = \left[\ln \left(\frac{z_1}{z_{0m}} \right) \right]^2 \left[\ln \left(\frac{z_1}{z_{0h}} \right) \right]^{-1} Ri_b (1 + 4.7 Ri_b) \quad (14)$$

The modified formula proposed by Brutsaert (1982) is used for calculation of roughness length for heat:

$$z_{0h} = z_{0m} / \exp(3.0(z_{0m} \cdot u_* / \nu_a)^{0.25} - 2.0) \quad (15)$$

where ν_a is the air kinematic molecular viscosity.

Finally, the sensible heat flux Q_H [$\text{W} \cdot \text{m}^{-2}$] and momentum flux Q_τ [$\text{N} \cdot \text{m}^{-2}$] are defined as:

$$Q_H = c_p \cdot \rho_a \cdot \overline{w'T'} \quad (16)$$

$$Q_\tau = \rho_a \cdot u_*^2 \quad (17)$$

where c_p is air specific heat at constant pressure [$\text{J} \cdot \text{kg}^{-1} \cdot \text{K}^{-1}$] and ρ_a – air density [$\text{kg} \cdot \text{m}^{-3}$].

Additionally, the turbulent atmospheric resistance for heat, r [$\text{s} \cdot \text{m}^{-1}$], is calculated as:

$$r = (T_{z_1} - T_{\text{Surf}}) / \overline{w'T'} \quad (18)$$

Water balance and latent heat flux

The latent heat flux is calculated using the bulk transfer and resistance concept:

$$\begin{aligned} Q_E &= L_v \cdot E = L_v \cdot \rho_a \cdot \overline{w'q'} = \\ &= L_v \cdot \rho_a \frac{(q_{\text{sat}}(T_{\text{Surf}}) - q_{z_1})}{r + r_s} \end{aligned} \quad (19)$$

where L_v – latent heat of vaporisation [$\text{J} \cdot \text{kg}^{-1}$], E – evapotranspiration [$\text{kg} \cdot \text{m}^{-2} \cdot \text{s}^{-1}$], $q_{\text{sat}}(T_{\text{Surf}})$ – saturated specific surface humidity as a function of surface temperature. The additional surface resistance r_s is assumed to be zero in the case of the water on the surface (Q_E equals potential

evaporation); otherwise, it is calculated using a method similar to that proposed by Best (1998):

$$r_s = \min \left\{ \frac{r_{s,\min}}{f_s \cdot f_M \cdot f_e \cdot f_T}, r_{s,\max} \right\} \quad (20)$$

The minimum, $r_{s,\min}$, and maximum, $r_{s,\max}$, are set as 40 and $5 \cdot 10^4 \text{ s} \cdot \text{m}^{-1}$. The functions for solar radiation, f_s , soil moisture content, f_M , vapour pressure deficit, f_e , and temperature, f_T , are defined as follows:

– the function for solar radiation f_s (Dolman *et al.* 1991):

$$f_s = 1.25 \left(\frac{S_d}{S_d + a_1} \right) \quad (21)$$

where S_d means total downward shortwave radiation [$\text{W} \cdot \text{m}^{-2}$] and $a_1 = 250 \text{ W} \cdot \text{m}^{-2}$,

– the function for soil moisture content, f_M (Dickinson *et al.* 1991):

$$f_M = \begin{cases} 1.0 & \text{if } \text{SMC} \geq 0.5 \\ 2 \times \text{SMC} & \text{if } \text{SMC} < 0.5 \end{cases} \quad (22)$$

– the function for vapour pressure deficit, f_e (Dickinson *et al.* 1991):

$$f_e = 1.0 - \frac{\Delta e_a}{\Delta e_a + a_2} \quad (23)$$

where $\Delta e_a = e_{\text{sat}}(T_{\text{surf}}) - e_{z1}$ is the vapour pressure deficit [hPa] and $a_2 = 30 \text{ hPa}$,

– the function for temperature, f_T (Dickinson *et al.* 1991):

$$f_T = \max\{a_3 \cdot T_{z1} \cdot (a_4 - T_{z1}), 0.04\} \quad (24)$$

where T_{z1} is air temperature [$^{\circ}\text{C}$] and $a_3 = 1.6 \cdot 10^{-3}$, $a_4 = 50^{\circ}\text{C}$. The minimum value of f_T is set to 0.04 to avoid zero Q_E flux at low temperatures.

The water balance (in the absence of snow cover) is calculated on the assumption that only a thin layer of the surface slab, with a thickness G_p [m], is directly subjected to precipitation/evaporation processes that alter its moisture content, SMC. If water is present at the surface, it is assumed to completely cover the surface plate with a thin layer of W_s [m], with a maximum thickness of $W_{s,\max}$. Depending on whether or not there is a liquid water layer on the surface the SMC changes in each iteration step, ΔSMC , are calculated as:

$$\Delta\text{SMC} = \begin{cases} -E \cdot \Delta t / (q_w \cdot G_p) & \text{if } W_s = 0 \\ I_R \cdot \Delta t / G_p & \text{if } 0 < W_s < W_{s,\max} \\ (I_R \cdot \Delta t + W_s - W_{s,\max}) / G_p & \text{if } W_s \geq W_{s,\max} \end{cases} \quad (25)$$

where I_R is a infiltration rate [$\text{m} \cdot \text{s}^{-1}$] ($I_R = \min\{a_{IR} \cdot W_s, I_{R,\max}\}$ with $a_{IR} = 8.33 \cdot 10^{-4} \cdot \text{s}^{-1}$ and $I_{R,\max} = 1.0 \cdot 10^{-4} \text{ m} \cdot \text{s}^{-1}$, q_w – water density [$\text{kg} \cdot \text{m}^{-3}$]. The last line in the above equation represents a rapid increase in SMC under heavy rainfall. In addition, the maximum, SMC_{\max} , and minimum, SMC_{\min} , values of SMC are set as site-specific parameters. Those parameters are estimated separately, taking into consideration the surface characteristics that determine properties of the surface slab (e.g., fractions of the area of impervious surface, trees, grass, bare soil and water surface). The SMC_{\min} determines Q_E at equilibrium when the direct effect of precipitation vanishes. Physically, this can be interpreted as the formation of water flux from deeper layers during the dry period and/or constant anthropogenic water supply of urban slab, which maintain the surface layer moisture at the minimum level. The SMC_{\max} determines the water storage capacity of the surface slab and, in combination with G_p , it is responsible for the rate of recession of Q_E to equilibrium. To include the effect of a long-term dry/wet period on evapotranspiration, the SMC_{\min} is assumed to vary slowly depending on cumulative precipitation:

$$\text{SMC}_{\min} = \text{SMC}_{\min} (1 - 0.5(\Delta t / t_{\text{yr}}) \cdot (1 - P_{\Delta t} / P_{\text{yr}})) \quad (26)$$

where t_{yr} is the period of 365 days in seconds, Δt – iteration step [s], $P_{\Delta t}$ – precipitation (rainfall + snowfall) in iteration step P_{yr} – mean (climatological) annual precipitation total for the selected location. This equation means that the SMC_{\min} can drop by half within the year if the annual sum of precipitation is zero. Moreover, it is assumed that the SMC_{\min} cannot be greater than 0.6 SMC_{\max} .

The change in surface water in each iteration step is determined by precipitation, infiltration and evapotranspiration:

$$\Delta W_s = (R_f - E - q_w \cdot I_R) \Delta t / q_w \quad (27)$$

If the level of the water on the surface, W_s , exceeds the fixed maximum value $W_{s,\max}$ it is assumed to be removed by runoff processes

at the end of each iteration. Thus, the runoff intensity, R_{runoff} [$\text{kg}\cdot\text{m}^{-2}\cdot\text{s}^{-1}$], is defined as:

$$R_{\text{runoff}} = R_f - E - \Delta\text{SMC} \cdot G_p \cdot q_w / \Delta t \quad (28)$$

Then the water level on the surface is lower than potential evaporation Q_E is calculated as a weighted mean of potential evaporation (Q_E for $r_s = 0$) and actual evapotranspiration (Q_E for $r_s > 0$), with weights proportional to the ratio of energy used to evaporate actual water to the energy of potential evaporation.

The modelling of the heat balance in the presence of snow assumes that the snow forms a uniform layer that completely covers the surface slab. The model does not account for the presence of snow in isolated patches. However, in the case of a relatively limited amount of snow, it is assumed that it covers the surface slab for only a portion of the time step, which is consistent with the structure of the patches. Moreover, it is possible that a thin layer of liquid water covers the snow layer. The single snow layer with a depth D_S [m] and temperature T_{Snow} is analysed. This physical snow depth is assumed to be ten times the water-equivalent snow depth (Chen, Dudhia 2001). The additional heat flux from the snow layer to the ground is considered to be:

$$Q_{\text{SG}} = \frac{2(T_{\text{Snow}} - T_{\text{G,1}})}{D_S/k_{\text{Snow}} + d_1/k_g} \quad (29)$$

Although the thermal diffusivity for snow, k_{Snow} , depends on the porosity of the snow, it is set to be $0.35 \text{ W}\cdot\text{m}^{-1}\cdot\text{K}^{-1}$ in the present model. When there is snow cover, the snow temperature is taken as a surface temperature and snow albedo and emissivity are used in radiation balance. Additional heat used for melting/freezing processes is considered.

In the event of snowfall or snow cover on the surface, the water balance and Q_E are calculated separately for the following cases:

1. There is no melting process and no liquid water on the surface (i.e., available energy is less than needed to warm snow to the melting temperature and no liquid water on the surface):
 - 1.1. The surface is covered by snow during the whole iteration period: Q_E is calculated as a potential evaporation from snow; the snow albedo and emissivity are taken for calculations of upward shortwave, K_u , and longwave, L_u , radiation.
 - 1.2. The surface is covered by snow during part of the iteration period: the above characteristics (Q_E , K_u , L_u) are calculated

as weighted means, with weights proportional to the ratio of energy used for snow evaporation to the potential evaporation energy.

2. Melting is taking place, or a liquid water and snow layers exists on the surface; some liquid water infiltrate the ground and some evaporate:

- 2.1. All the snow melts: the energy used for melting snow is subtracted from the heat balance, and then the scheme for water balance with surface water formed by melting snow is applied. The K_u and L_u are calculated as weighted means with albedo and emissivity for snow and bare surface, using weights proportional to the ratio of energy used to melt snow to the total available energy.

- 2.2. Not all the snow melts:

- 2.2.1. Not all surface water (liquid + snow) evaporates: Q_E is calculated as a weighted mean of potential evaporation from water and snow; snow albedo and emissivity are used in K_u and L_u calculations.

- 2.2.2. All surface water (liquid + snow) evaporates: Q_E is calculated as a weighted mean of potential evaporation from water and snow (Q_E for $r_s = 0$) and actual evapotranspiration (Q_E for $r_s > 0$); similarly, K_u and L_u are calculated as weighted means with albedo and emissivity for snow and bare surface. Weights are proportional to the energy used for each process.

Experimental data used for validation

Data from two eddy-covariance measurement sites, representing urban and wetland conditions, were selected for preliminary model validation. The urban site was located at 81 Lipowa St. in Lodz, central Poland ($51^\circ 45' 45''\text{N}$, $19^\circ 26' 43''\text{E}$, 204 m a.s.l.) in the western part of the densely built-up city centre. The immediate vicinity of the site is characterised by compact development. In this part of the city, artificial surfaces (buildings, roads, pavements, etc.) cover ~50–70% of the surface. Vegetation (mainly small lawns) covers 38% of the total area and is interspersed with buildings. The data were collected on a thin mast, 20 m in height, located on the roof of a 17-m-tall building. The measurement height was thus 37 m above ground level, which is more

than twice the height of the canopy. The buildings surrounding the site are of similar height to the trees, resulting in a well-formed urban canopy with an average height $z_H = 11$ m. Therefore, it can be assumed that the measurements were made above the roughness layer. Based on the simple rule of thumb $z_d = 0.7z_H$, the displacement height z_d is estimated to be 7.7 m. The roughness length for the momentum around the measurement site averaged $z_{0m} = 1.7$ m. More information on the site, the city's structure and the local climate conditions can be found in, e.g. Offerle *et al.* (2006), Pawlak *et al.* (2011, 2016), Fortuniak *et al.* (2013), Fortuniak, Pawlak (2015). The present study uses data from 2009.09.11 to 2014.07.26.

The wetland site (53°35'30"N, 22°53'32"E, 109 m a.s.l.) was located in north-eastern Poland in the Middle Biebrza Basin of the Biebrza National Park near the village of Kopytkowo. The vegetation in the source area of the eddy-covariance system was dominated by a mixture of sedges, reeds and rushes, which is typical for the wetlands of the Biebrza River. Mean vegetation height varied from ~0.8 m in the western sector (mainly covered by sedges) to ~2.0 m in the eastern sector (mainly covered by reeds). The measurement height was 3.7 m above ground. The roughness length for the momentum around

the measurement site averaged $z_{0m} = 0.15$ m. See Fortuniak *et al.* (2017, 2021) and Pawlak *et al.* (2016) for a detailed description of the site, instrumentation and data proceedings. The data used in this study cover the period from 2021.01.01 to 2022.12.31.

Results and discussion

The choice of physical parameters that characterise the surface slab is crucial to the simulation results. The presented simulations for urban site used the same parameters as in the Urban-PLUMBER project (Lipson *et al.* 2023). The radiative and dynamic parameters were set using experimental data: $\alpha = 0.09$, $\varepsilon = 0.09$, $z_{0m} = 1.7$ [m], while the thermo-moisture parameters $C_g = 1.95 \cdot 10^6$ [$J \cdot m^{-3} \cdot K^{-1}$], $k_g = 0.85$ [$W \cdot m^{-1} \cdot K^{-1}$], $SMC_{min} = 0.05$, $SMC_{max} = 0.19$ were adjusted as a weighted average of typical tile parameters (Tab. 1), with weights proportional to the fractions of the major surface coverages: impervious surfaces, trees, grass, bare soil, water surfaces. Such an approach is the result of a comparison of different cities in the second phase of the project. Thus, these parameters are not optimised for the Lipowa location, which may reduce the accuracy of the simulation, but at the same time makes the results more universal.

Table 1

Soil parameters for various surface coverages used to estimate urban slab parameters

	$C_g \times 10^6$ [$J \cdot m^{-3} \cdot K^{-1}$]	k_g [$W \cdot m^{-1} \cdot K^{-1}$]	SMC_{min}	SMC_{max}
impervious surfaces	2.20	1.00	0.00	0.00
trees	1.00	0.20	0.20	0.80
grass	1.50	0.70	0.18	0.80
bare soil	2.00	1.00	0.05	0.50
water surfaces	4.20	0.55	1.00	1.00

For the wetland site, the thermal parameters characteristic of partially dry peat were chosen as $C_g = 1.90 \cdot 10^6$ [$J \cdot m^{-3} \cdot K^{-1}$] and $k_g = 0.15$ [$W \cdot m^{-1} \cdot K^{-1}$], and the soil moisture was set as $SMC_{min} = 0.40$ and $SMC_{max} = 0.99$. Empirical values were used for the radiative and dynamical

parameters: $\alpha = 0.18$, $\varepsilon = 0.9$, $z_{0m} = 0.15$ [m]. The simulations for both the urban and wetland sites assumed liquid precipitation and no snow cover, due to the unavailability of precipitation type and snow cover information.

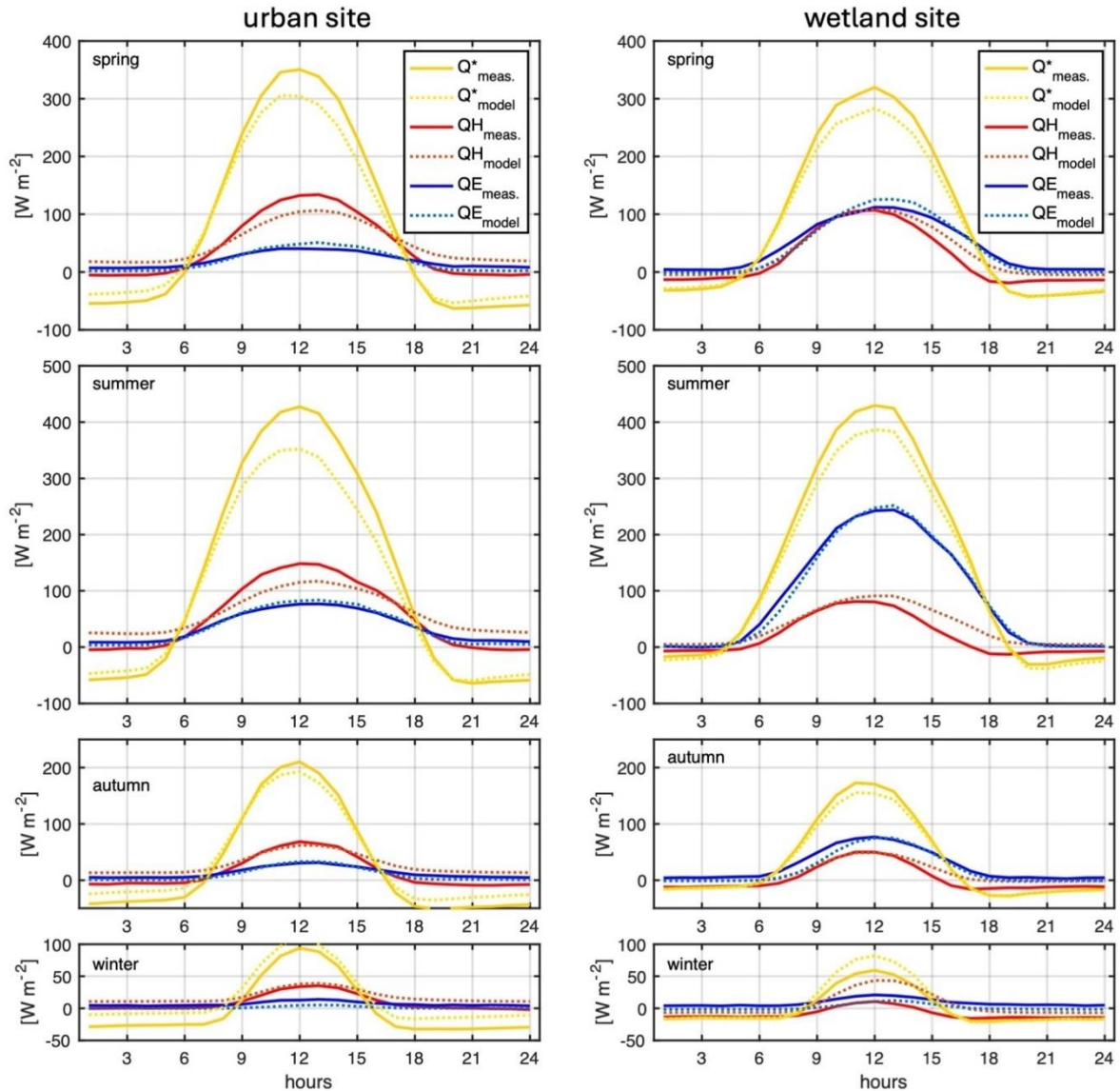


Fig. 1. Modelled and measured mean diurnal course of the energy balance component in the seasons for the urban site and the wetland site

The modelled and measured averaged daily courses of the energy balance components in the seasons are shown in Figure 1 and the corresponding fit statistics in Table 2. In general, at both the urban and wetland sites, the model correctly captures the main features of the diurnal pattern of the heat balance components. The dominance of sensible heat over latent heat during daylight hours, characteristic of urban areas, is clearly visible. However, midday Q_H values are clearly underestimated in spring and summer, while nighttime values are overestimated in all seasons. Contrary to Q_H , the radiation balance is underestimated during the day and overestimated during the night, except in winter, which is a consequence

of the excessive amplitude of the modelled upward longwave radiation. In contrast, the diurnal evolution of the latent heat flux is surprisingly well reproduced by the model.

In the case of the wetland site, the model performs slightly better. The latent heat flux is significantly higher than the sensible heat flux, which is particularly pronounced in the summer months. With the exception of winter, the highest values of modelled Q_H and Q_E are very similar to measured ones. However, in the afternoon, the modelled sensible heat flux is higher than the measured one. The radiation balance values in the midday hours are, as in urban areas, underestimated by the model.

Table 2

Model fit statistics for measured data for hourly mean values of the energy balance components for the urban site and the wetland site in the seasons

Explanations: mean bias error (MBE [$W \cdot m^{-2}$]), mean absolute error (MAE [$W \cdot m^{-2}$]), root mean squared error (RMSE [$W \cdot m^{-2}$]), Willmott's goodness of fit (d), and coefficient of determination (R^2)

	urban site					wetland site				
	MBE	RMSE	MAE	d	R^2	MBE	RMSE	MAE	d	R^2
Spring										
Q^*	-6.2	24.5	20.3	0.993	0.997	-10.0	17.8	12.1	0.995	0.999
Q_H	6.2	21.1	19.6	0.939	0.988	9.9	12.9	10.4	0.979	0.971
Q_E	-1.4	6.0	5.6	0.963	0.986	-2.1	8.9	7.7	0.990	0.982
Summer										
Q^*	-21.3	39.0	28.8	0.987	0.997	-16.2	21.6	16.2	0.996	0.999
Q_H	6.1	25.1	23.0	0.927	0.982	15.4	18.2	15.4	0.929	0.920
Q_E	-0.8	4.9	4.5	0.993	0.998	-1.7	7.0	4.5	0.999	0.995
Autumn										
Q^*	7.7	14.8	13.9	0.992	0.999	-4.4	7.4	4.5	0.997	0.999
Q_H	13.6	17.0	15.1	0.872	0.989	9.3	10.7	9.5	0.934	0.973
Q_E	-3.0	4.0	3.8	0.964	0.985	-6.1	7.9	6.5	0.979	0.967
Winter										
Q^*	16.5	16.7	16.5	0.962	0.997	5.1	9.6	5.5	0.976	0.999
Q_H	9.2	9.6	9.2	0.853	0.988	14.0	17.2	14.0	0.673	0.915
Q_E	-5.7	5.9	5.7	0.511	0.960	-7.0	7.1	7.0	0.674	0.955

Similar conclusions can be drawn from an analysis of monthly averages (Fig. 2, Tab. 3). The model performs well in the case of latent heat flux and overestimates sensible heat flux. The radiation balance is underestimated in summer and overestimated in winter. The fact that the model works quite well for Q_E and worse for Q_H is also confirmed by comparing the measured

and modelled values of Q_H and Q_E (Fig. 3). The sensible heat flux is generally overestimated at low values and underestimated at high values, and the relationship is not linear. The effect is more pronounced at the urban site (where higher Q_H values are typically observed) than at the wetland site.

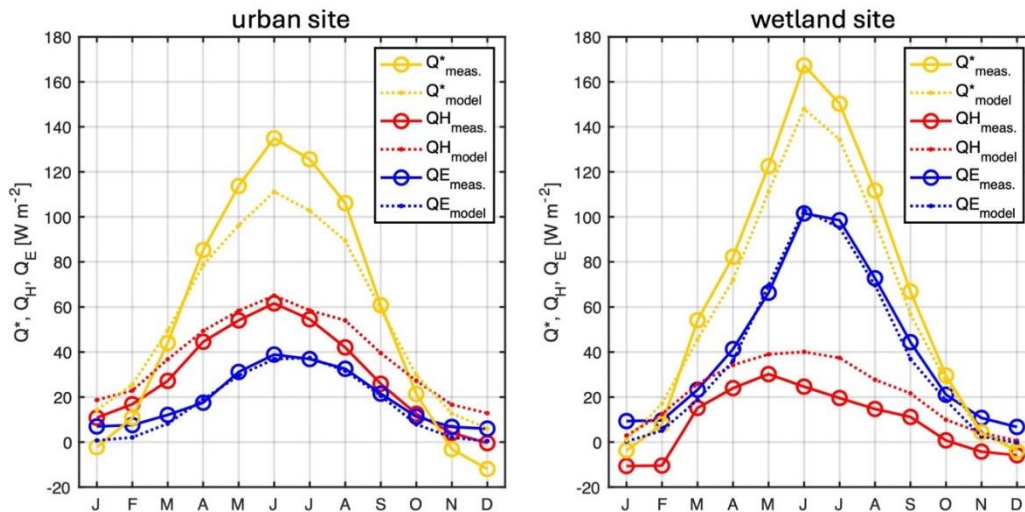


Fig. 2 Modelled and measured monthly means of the energy balance component for the urban site and the wetland site

Table 3

Model fit statistics for measured data for monthly means of the energy balance components for the urban site and the wetland site

Explanations: mean bias error (MBE [$\text{W}\cdot\text{m}^{-2}$]), mean absolute error (MAE [$\text{W}\cdot\text{m}^{-2}$]), root mean squared error (RMSE [$\text{W}\cdot\text{m}^{-2}$]), Willmott's goodness of fit (d), and coefficient of determination (R^2)

	urban site					wetland site				
	MBE	RMSE	MAE	d	R^2	MBE	RMSE	MAE	d	R^2
Q^*	-0.8	15.5	14.0	0.970	0.998	-6.4	10.6	9.0	0.991	0.996
Q_H	8.8	9.7	8.8	0.938	0.974	12.3	13.0	12.3	0.821	0.903
Q_E	-2.7	3.6	3.0	0.981	0.986	-4.2	5.5	5.0	0.994	0.995

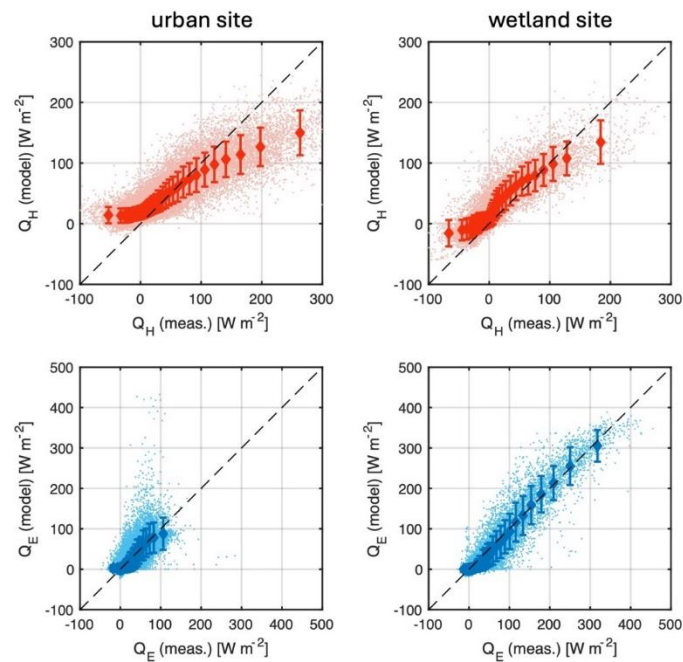


Fig. 3. Modelled against the observed sensible heat flux (Q_H) and latent heat flux (Q_E) for the urban site and the wetland site.

All available (light dots) and bin-averaged (mean \pm standard deviation – dark diamonds) data

Concluding remarks

The presented scheme belongs to the simple approaches to parametrisation of the surface energy balance. This is not only due to the slab approach itself, but also because the tile parameters remain constant over time and uniform across all layers. Allowing these parameters to vary might improve the model. For example, the thermal properties of the soil could be set to depend on moisture content or vary with the seasons. In addition, the model assumes that the radiation exchange surface is flat and completely opaque. This results in large temperature gradients in soil and can consequently affect the sensible heat flux. In fact, for both urbanised areas and most natural ecosystems, the surface slab is more like a porous me-

dium, in which radiation is absorbed/emitted through a process of multiple reflections in a layer of a certain thickness. Therefore, it would be more natural to assume that the surface is semi-opaque and that the exchange of radiation does not only take place through a thin layer of the flat active surface.

Nevertheless, the implementation of such enhancements might reduce model efficacy by increasing the number of computational operations involved. The current model is characterised by a fairly fast performance while reproducing the basic features of the heat balance across a range of surface types, as exemplified in the presented case. Without increasing the complexity, the quality of the simulation can be improved by optimising the parameters of the surface slab.

In the present simulation, these parameters were estimated based on the physical properties of various soils and materials. Instead, the porous-like nature of urban and wetland ecosystems suggests that the properties of their slabs may diverge considerably from those of solid materials.

It is also noteworthy that, as demonstrated by Grimmond *et al.* (2009, 2010, 2011) and Lipson *et al.* (2023), despite the mentioned limitations, the presented scheme exhibits comparable performance to more complex algorithms. When considered alongside numerical efficiency, this proves the significant potential of slab models.

Acknowledgements

The authors thank the authorities of the Biebrza National Park for allowing the continuous measurements in the area of the Park. Furthermore, we would like to thank Mrs and Mr Raczkowski of the agritourist farm “Dworek na końcu świata” for their guardianship. Funding for this research was provided by the National Science Centre, Poland under project UMO-2020/37/B/ST10/01219 and University of Lodz under project 4/IDUB/DOS/2021.

References

- Best M.J. 1998. A Model to Predict Surface Temperatures. *Boundary-Layer Meteorology* 88(2): 279-306.
<https://doi.org/10.1023/A:1001151927113>
- Brutsaert W. 1982. *Evaporation into the Atmosphere*. Springer Netherlands.
<https://doi.org/10.1007/978-94-017-1497-6>
- Chen F., Dudhia J. 2001. Coupling and advanced land surface-hydrology model with the Penn State-NCAR MM5 modeling system. Part I: Model implementation and sensitivity. *Monthly Weather Review* 129(4): 569-585.
[https://doi.org/10.1175/1520-0493\(2001\)129<0569:CAALSH>2.0.CO;2](https://doi.org/10.1175/1520-0493(2001)129<0569:CAALSH>2.0.CO;2)
- Cheval S., Amihăesei V.A., Chitu Z., Dumitrescu A., Falcescu V., Iraşoc A., Micu D.M., Mihulet E., Ontel I., Paraschiv M.G., Tudose N.C. 2024. A systematic review of urban heat island and heat waves research (1991–2022). *Climate Risk Management* 44: 100603.
<https://doi.org/10.1016/j.crm.2024.100603>
- Dickinson R.E., Henderson-Sellers A., Rosenzweig C., Sellers P.J. 1991. Evapotranspiration models with canopy resistance for use in climate models, a review. *Agricultural and Forest Meteorology* 54(2–4): 373-388.
- Dolman A.J., Gash J.H.C., Roberts J., Shuttleworth W.J. 1991. Stomatal and surface conductance of tropical rainforest. *Agricultural and Forest Meteorology* 54(2–4): 303-318.
- Fortuniak K. 2003. A slab surface energy balance model (SUEB) and its application to the study on the role of roughness length in forming an urban heat island. *Acta Universitatis Wratislaviensis – Studia Geograficzne* 75: 368-377.
- Fortuniak K., Pawlak W. 2015. Selected Spectral Characteristics of Turbulence over an Urbanized Area in the Centre of Łódź, Poland. *Boundary-Layer Meteorology* 154(1): 137-156.
- Fortuniak K., Pawlak, W., Siedlecki M. 2013. Integral Turbulence Statistics Over a Central European City Centre. *Boundary-Layer Meteorology* 146(2): 257-276.
<https://doi.org/10.1007/s10546-012-9762-1>
- Fortuniak K., Pawlak W., Siedlecki M., Chambers S., Bednorz L. 2021. Temperate mire fluctuations from carbon sink to carbon source following changes in water table. *Science of the Total Environment* 756.
<https://doi.org/10.1016/j.scitotenv.2020.144071>
- Fortuniak K., Pawlak W., Bednorz L., Grygoruk M., Siedlecki M., Zieliński M. 2017. Methane and carbon dioxide fluxes of a temperate mire in Central Europe. *Agricultural and Forest Meteorology* 232: 306-318.
<https://doi.org/10.1016/j.agrformet.2016.08.023>
- Grimmond C.S.B., Best M., Barlow J., Arnfield A.J., Baik J.J., Baklanov A., Belcher S., Bruse M., Calmet I., Chen F., Clark P., Dandou A., Erell E., Fortunia, K., Hamdi R., Kanda M., Kawai T., Kondo H., Krayenhoff S., Williamson T. 2009. Urban Surface Energy Balance Models: Model Characteristics and Methodology for a Comparison Study. In *Meteorological and Air Quality Models for Urban Areas*. Springer Berlin Heidelberg: 97-123.
- Grimmond C.S.B., Blackett M., Best M.J., Barlow J., Baik J.J., Belcher S.E., Bohnenstengel S.I., Calmet I., Chen F., Dandou A., Fortuniak K., Gouvea M.L., Hamdi R., Hendry M., Kawai T., Kawamoto Y., Kondo H., Krayenhoff E.S., Lee S.H., Zhang N. 2010. The international urban energy balance mod-

- els comparison project: First results from phase 1. *Journal of Applied Meteorology and Climatology* 49(6): 1268-1292.
<https://doi.org/10.1175/2010JAMC2354.1>
- Grimmond C.S.B., Blackett M., Best M.J., Baik J.J., Belcher S.E., Beringer J., Bohnenstengel S.I., Calmet I., Chen F., Coutts A., Dandou A., Fortuniak K., Gouvea M.L., Hamdi R., Hendry M., Kanda M., Kawai T., Kawamoto Y., Kondo H., Zhang N. 2011. Initial results from Phase 2 of the international urban energy balance model comparison. *International Journal of Climatology* 31(2): 244-272.
<https://doi.org/10.1002/joc.2227>
- Ho J.Y., Shi Y., Lau K.K.L., Ng E.Y.Y., Ren C., Goggins W.B. 2023. Urban heat island effect-related mortality under extreme heat and non-extreme heat scenarios: A 2010–2019 case study in Hong Kong. *Science of The Total Environment* 858: 159791.
- IPCC. 2024. Climate Change 2022: Mitigation of Climate Change. Contribution of Working Group III to the Sixth Assessment Report of the Intergovernmental Panel on Climate Change. In *Cambridge University Press* (Issue 1). Online: <https://www.ipcc.ch/report/ar6/wg3/> (last access: 09.01.2024).
- Lipson M.J., Grimmond S., Best M., Abramowitz G., Coutts A., Tapper N., Baik J., Beyers M., Blunn L., Boussetta S., Bou-Zeid E., De Kauwe M.G., de Munck C., Demuzere M., Faticchi S., Fortuniak K., Han B., Hendry M.A., Kikegawa Y., Pitman A.J. 2023. Evaluation of 30 urban land surface models in the <scp>Urban-PLUMBER</scp> project: Phase 1 results. *Quarterly Journal of the Royal Meteorological Society*.
<https://doi.org/10.1002/qj.4589>
- Lwasa S.K., Seto C., Bai X., Blanco H., Gurney K.R., Kılıç Ş., Lucon O., Murakami J., Pan J., Sharifi A., Yamagata Y. 2022. Urban systems and other settlements. In: P.R. Shukla, J. Skea, R. Slade, A. Al Khourdajie, R. van Diemen, D. McCollum, M. Pathak, S. Some, P. Vyas, R. Fradera, M. Belkacemi, A. Hasija, G. Lisboa, S. Luz, J. Malley (eds.) *Climate Change 2022: Mitigation of Climate Change. Contribution of Working Group III to the Sixth Assessment Report of the Intergovernmental Panel on Climate Change*: 861-952.
- Mascart P., Noilhan J., Giordani H. 1995. A modified parameterization of flux-profile relationships in the surface layer using different roughness length values for heat and momentum. *Boundary-Layer Meteorology* 72(4): 331-344.
<https://doi.org/10.1007/BF00708998>
- Nazarian N., Lipson M., Norford L.K. 2023. Multiscale modeling techniques to document urban climate change. In: *Urban Climate Change and Heat Islands*. Elsevier: 123-164.
<https://doi.org/10.1016/B978-0-12-818977-1.00004-1>
- Offerle B., Grimmond S., Fortuniak K., Klyzik K., Oke T.R. 2006. Temporal variations in heat fluxes over a central European city centre. *Theoretical and Applied Climatology* 84(1–3): 103-115.
- Oke T.R. 1973. City size and the urban heat island. *Atmospheric Environment (1967)* 7(8): 769-779.
- Oke T.R. 1982. The energetic basis of the urban heat island. *Quarterly Journal of the Royal Meteorological Society* 108(455): 1-24.
<https://doi.org/10.1002/qj.49710845502>
- Pawlak W., Fortuniak K., Siedlecki M. 2011. Carbon dioxide flux in the centre of Łódź, Poland-analysis of a 2-year eddy covariance measurement data set. *International Journal of Climatology* 31(2): 232-243.
<https://doi.org/10.1002/joc.2247>
- Pawlak W., Fortuniak K., Siedlecki M., Zieliński M. 2016. Urban – Wetland contrast in turbulent exchange of methane. *Atmospheric Environment* 145: 176-191.
- Rosenzweig C., Solecki W.D., Romero-Lankao P., Mehrotra S., Dhakal S., Ali Ibrahim S. (eds.). 2018. *Climate Change and Cities*. Cambridge University Press.
<https://doi.org/10.1017/9781316563878>
- Seto K.S., Dhakal S., Bigio A., Blanco H., Delgado G.C., Dewar D., Huang L., Inaba A., Kansal A., Lwasa S., McMahon J.E., Müller D.B., Murakami J., Nagendra H., Ramaswami A. 2014. Human Settlements, Infrastructure and Spatial Planning. In: O. Edenhofer, R. Pichs-Madruga, Y. Sokona, E. Farahani, S. Kadner, K. Seyboth, A. Adler, I. Baum, S. Brunner, P. Eickemeier, B. Kriemann, J. Savolainen, S. Schlömer, C. von Stechow, T. Zwickel, J.C. Minx (eds.) *Climate Change 2014: Mitigation of Climate Change. Contribution of Working Group III to the Fifth Assessment Report of the Intergovernmental Panel on Climate Change* Cambridge University Press. Cambridge, United Kingdom and New York, USA: 923-1000.